National Renewable Energy Laboratory
A national laboratory of the U.S. Department of Energy
Office of Energy Efficiency & Renewable Energy
Innovation for Our Energy Future

Rotational Augmentation Disparities in the MEXICO and UAE Phase VI Experiments

Preprint

S. Schreck
National Renewable Energy Laboratory

T. Sant
University of Malta

D. Micallef
University of Malta and Technical University of Delft

To be presented at the 2010 Torque from Wind Conference
Heraklion, Greece
June 28-30, 2010

Conference Paper
NREL/CP-500-47759
May 2010

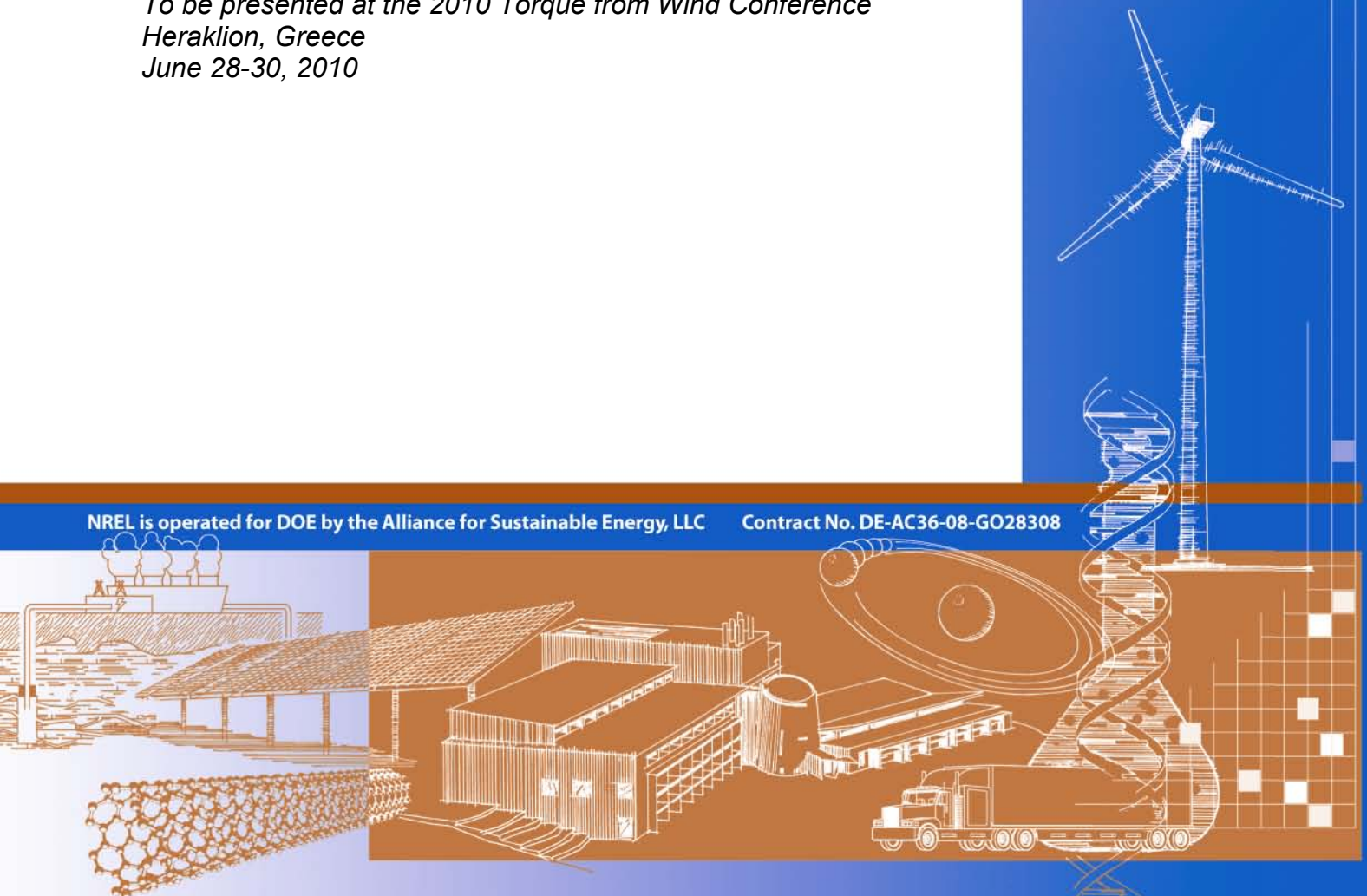

NREL is operated for DOE by the Alliance for Sustainable Energy, LLC Contract No. DE-AC36-08-GO28308

Available electronically at http://www.osti.gov/bridge

Available for a processing fee to U.S. Department of Energy
and its contractors, in paper, from:

U.S. Department of Energy
Office of Scientific and Technical Information
P.O. Box 62
Oak Ridge, TN 37831-0062
phone: 865.576.8401
fax: 865.576.5728
email: mailto:reports@adonis.osti.gov

Available for sale to the public, in paper, from:

U.S. Department of Commerce
National Technical Information Service
5285 Port Royal Road
Springfield, VA 22161
phone: 800.553.6847
fax: 703.605.6900
email: orders@ntis.fedworld.gov
online ordering: http://www.ntis.gov/ordering.htm

Printed on paper containing at least 50% wastepaper, including 20% postconsumer waste

Rotational Augmentation Disparities in the MEXICO and UAE Phase VI Experiments

S. Schreck
Nat'l Renewable Energy Laboratory
Nat'l Wind Technology Center
1617 Cole Blvd.
Golden, CO 80027
United States
scott.schreck@nrel.gov

T. Sant
University of Malta
Faculty of Engineering
Room 315 MSD
2080 Malta
tonio.sant@um.edu.mt

D. Micallef
Technical University of Delft
University of Malta
Faculty of Engineering
Room 217 MSD
2080 Malta
d.micallef@tudelft.nl

Abstract

Wind turbine structures and components suffer excessive loads and premature failures when key aerodynamic phenomena are not well characterized, fail to be understood, or are inaccurately predicted. Turbine blade rotational augmentation remains incompletely characterized and understood, thus limiting robust prediction for design. Pertinent rotational augmentation research including experimental, theoretical, and computational work has been pursued for some time, but large scale wind tunnel testing is a relatively recent development for investigating wind turbine blade aerodynamics. Because of their large scale and complementary nature, the MEXICO and UAE Phase VI wind tunnel experiments offer unprecedented synergies to better characterize and understand rotational augmentation of blade aerodynamics. C_n means, C_n standard deviations, two-dimensional c_p distributions, and three-dimensional planform surface pressure topologies from these two experiments were analyzed and compared. Rotating blade data were evaluated against analogous stationary blade data. Rotational augmentation effects were found to be pervasive and were present over the blade radius and throughout blade operating envelopes at all radial locations investigated. Rotational effects manifested themselves in both mean and time varying statistics, in both two-dimensional sectional data as well as three-dimensional planform data. Comparative analyses of MEXICO and UAE data validated and generalized current knowledge regarding rotationally augmented blade flow fields. In addition to confirming prior research, results also provided new insights not attainable by considering either data set in isolation of the other.

Keywords: Force amplification, rotational augmentation, wind tunnel, wind turbine, unsteady loading

1 Introduction

Wind turbine service life is shortened and operability curtailed when unanticipated aerodynamic loads impose excessive stresses on wind turbine structural and mechanical components. Failure to accurately predict turbine aerodynamic loads is due largely to the complex nature of wind turbine blade aerodynamics and incomplete comprehension of the underlying fluid dynamics. At present, key wind turbine aerodynamic phenomena remain incompletely characterized and understood.

Historically, experimentation and testing have occupied a central role in discovering, characterizing, and understanding fluid dynamic phenomena that govern wind turbine power production and structural loading. Early field experiments were carried out concurrently at the Netherlands Energy Research Foundation, Delft University of Technology, National Renewable Energy Laboratory, Risoe Wind Turbine Test Station, and Imperial College. Notably, these efforts successfully carried out research grade measurements of turbine aerodynamics and structural dynamics in the challenging field environment. These efforts were documented through IEA Wind Annex XIV [1] and Annex XVIII [2].

Unfortunately, the accurate, detailed measurements acquired in these field experiments accentuated a long standing dilemma. Large scale turbine geometries could be densely instrumented and successfully tested, but the uncontrollable and sparsely characterized atmospheric inflows introduced overriding uncertainties. Alternatively, wind tunnel testing offered controlled and uniform inflows, but test section dimensions constrained turbine size, leading to severe mismatches in Reynolds number and other similarity parameters. These uncontrolled inflows and similarity parameter disparities were broadly recognized as significant impediments to deeper comprehension and more accurate prediction of turbine aerodynamics.

This dilemma was first addressed by a series of joint projects between the Aeronautical Research Institute of Sweden (FFA) and the China Aerodynamics Research and Development Center (CARDC). This series of projects culminated in 1990, when testing was completed in the CARDC 12 m x 16 m wind tunnel on a two-bladed rotor with a diameter of 5.35 m. In addition to nacelle and blade root moments, surface pressures were measured at 232 taps distributed over eight radial stations.[3,4] Success in these experiments stimulated interest internationally, and laid the foundations for more ambitious plans involving still larger turbines and wind tunnels, and more elaborate test protocols.

Resource constraints and facility schedules postponed further wind tunnel testing of larger scale wind turbines until the following decade. In 2000, NREL completed testing of the 10.1 m diameter Unsteady Aerodynamics Experiment (UAE) Phase VI turbine in the NASA Ames 24.4 m x 36.6 m wind tunnel.[5] In 2006, EU Model Rotor Experiment in Controlled Conditions (MEXICO) Project with a 4.5 m diameter rotor was tested in the DNW 9.5 m x 9.5 m LLF.[6] Notably, these efforts were sufficiently similar to enable corroborative comparisons, while specific differences showed effects not observed previously.

Wind tunnel testing of large scale turbines represents a crucial, though relatively recent development for understanding and predicting wind turbine aerodynamics. For rotational augmentation, prior research extends back some decades, encompassing experimental, theoretical, and computational work. A review of these efforts will not be undertaken herein, but can be found in previous documentation.[7] The current work will concentrate on characterizing and understanding rotational augmentation of blade aerodynamic response, using the aerodynamics measurements acquired in the MEXICO and UAE Phase VI wind tunnel tests.

2 Experimental Methods

2.1 MEXICO Turbine

MEXICO testing was carried out in the DNW LLF (Large Low-Speed Facility) 9.5 m x 9.5 m open jet, and has been documented by Snel, et al. [8,9] The MEXICO turbine had a three-bladed upwind rotor that was 4.5 m in diameter with zero cone angle. The rotor was pitch controlled and turned counterclockwise (viewed from downwind) at constant speed. Though the experiment encompassed multiple rotor speeds, data analyzed in the current work were acquired at a rotor speed of 325 RPM. A cylindrical tower 0.508 m in diameter with a spiral strake held the nacelle at a hub height of 5.12 m with 2.13 m overhang. This situated the rotor axis at the jet centerline and placed the rotor well upwind of the tower. The MEXICO turbine is shown in the left panel of Figure 1, in the DNW LLF 9.5 m x 9.5 m open jet.

Full pressure tap rows were located on all three blades, with the tap rows at 0.25R and 0.35R on blade 1, the 0.60R tap row on blade 2, and the 0.82R and 0.92R tap rows on blade 3. A full pressure tap row consisted of 25 to 28 taps, distributed over the blade pressure and suction surfaces. The upper part of Figure 2 shows the MEXICO pressure tap distribution on the blade suction surface, with all five full tap rows depicted on one blade. Pressure taps were more densely distributed near the blade leading edge to better resolve the pronounced gradients typically present there. To validate azimuthal uniformity, partial pressure tap rows were distributed over multiple blades at each radial location.

The MEXICO experiment blades were both twisted and tapered. The blade taper distribution is evident in Figure 2, with maximum blade chord being 0.240 m at 0.20R and tapering to 0.011 m at the tip. Figure 3 documents blade twist, which decreases from 16.4° at 0.20R to 0.0° at the tip. Between 0.20R and the tip, the blade cross section transitioned from the DU91-W2-250 airfoil ($0.20 \le r/R \le 0.46$), to the Risø A1-21 ($0.54 \le r/R \le 0.66$), and finally to the NACA 64-418 ($0.74 \le r/R \le 1.00$). The blade pitched about an axis located 0.25c aft of the leading edge, and centered between the blade upper and lower surfaces at that chord location.

Pressure taps were flush with the blade surface and 0.4 mm in diameter. Close coupled beneath each tap was a Kulite XCQ-95 series piezoresistive pressure transducer having sealed gage reference. Close coupling with the pressure taps minimized reduction of the transducers 150 kHz bandwidth, yielding flat frequency response across a broad spectrum. Each of the transducer pressure inputs was scanned at 5514 Hz. Test section flow speed and air properties were measured using the DNW LLF wind tunnel air data system.

Turbine blade plane of rotation was maintained orthogonal to the test section centerline, yielding a yaw angle of 0°. Blade pitch angle was held constant at -2.3°. Test section velocity (U_∞) was varied between 5.4 m/s and 30.0 m/s, at graduated intervals, yielding tip speed ratios (λ) of 14.1 to 2.5. At each U_∞, a 5 s data set was

acquired. Time records of c_p were integrated over the sectional chord to obtain time records of C_n. Time records of c_p and C_n were processed to obtain means and standard deviations for c_p and C_n.

2.2 UAE Phase VI Turbine

Several Phase VI UAE configurations were tested in the NFAC 24.4 m x 36.6 m wind tunnel, and are described by Hand, et al.[5] Data analyzed herein were acquired from a two bladed upwind rotor, 10.1 m in diameter, with zero cone angle. The rotor turned clockwise (viewed from downwind) at a constant 71.6 rpm, was stall regulated, and had a maximum rated power of 19.8 kW. A cylindrical tower 0.4 m in diameter supported the turbine at a hub height of 12.2 m (test section centerline), with 1.32 m rotor overhang. This UAE configuration, mounted in the NASA Ames 24.4 m x 36.6 m ft wind tunnel, is shown in the right panel of Figure 1.

The black blade on the left side of the rotor in Figure 1 was equipped with five full pressure tap rows to acquire detailed surface pressure data. A full pressure tap distribution consisted of 22 taps distributed over the pressure and suction surfaces of the blade. Pressure taps were more densely distributed near the blade leading edge to better resolve the pronounced gradients typically present there. The lower portion of Figure 2 shows that UAE full pressure tap distributions that were located at r/R = 0.30, 0.47, 0.63, 0.80, and 0.95.

The blades used throughout the NASA Ames wind tunnel test were both twisted and tapered. The blade taper distribution is apparent in Figure 2, with maximum blade chord being 0.737 m at 0.25R, and tapering to 0.356 m at the tip. Figure 3 documents blade twist, which decreases from 21.8° at 0.25R to 0.0° at the tip. Between 0.25R and the tip, blade cross section was uniform, corresponding to the S809 airfoil. The blade pitched about an axis located 0.30c aft of the leading edge, and centered between the blade upper and lower surfaces at that chord location. Design procedures, constraints, and measures of merit for this blade have been documented in detail.[10]

Surface pressure taps were flush mounted at the blade surface, and had inside diameters of 0.69 mm. From the taps, stainless steel hypodermic tubes with inside diameters of 0.69 mm transmitted surface pressures to the pressure transducers. Hypodermic tubing lengths were minimized to mitigate pressure delay and dispersion effects. Pressures were measured by five Pressure Systems Incorporated ESP-32 electronically scanned pressure transducers located inside the blade near the five full pressure tap distributions. Each of the transducer pressure inputs was scanned at 520.8 Hz. In conjunction with the tubing frequency response, this provided antialiased digitization and minimal gain variation out to 55 Hz.[11] Test section flow speed and air properties were measured using the 80 ft x 120 ft wind tunnel air data system described by Zell.[12]

All data were collected with the turbine rotating at a constant speed of 71.6 RPM. Turbine blade plane of rotation was maintained orthogonal to the test section centerline, yielding a yaw angle of 0°. Blade pitch angle was held constant at 3.0°. Test section velocity (U_∞)was varied between 5 m/s and 25 m/s, in nominal increments of 1 m/s, corresponding to tip speed ratios (λ) of 7.5 to 1.5. At each U_∞, a 30 s data record containing 36 blade rotation cycles was acquired. Time records of c_p were integrated over the sectional chord to obtain time records of C_n. Time records of c_p and C_n were processed to obtain means and standard deviations for c_p and C_n.

3 Results and Discussion

The results below compare MEXICO and UAE Phase VI sectional aerodynamic forces and surface pressure distributions, for radial locations near the blade root and farther out toward the blade tip. These analyses include both mean and time varying statistics. To provide some integration of sectional flow field characteristics, mean surface pressure topologies for select operating conditions also are included.

3.1 Local Inflow References

In both the MEXICO and UAE Phase VI experiments, local dynamic pressure was computed as the difference between test section static pressure (p_∞) and local total pressure (p_0). Local total pressure was determined at each full pressure tap distribution as the highest pressure sensed in the tap distribution.

An inverse free wake lifting line model was used to compute angles of attack (α) corresponding to the MEXICO and UAE Phase VI experimental data at zero yaw. This inverse free wake model has been thoroughly validated for both the UAE Phase VI [13] and MEXICO [14] databases. Thus, it furnished angle of attack data that were both accurate and consistent between the two experiments. It should be noted that the lifting line formulation limits the fidelity with which

three-dimensional flow field features are resolved at high angles of attack.

The pressure readings from the MEXICO experiment can yield the normal and tangential loads acting on the blades of the turbine for every spanwise location and azimuth angle at which the data are sampled. In the inverse free wake model, the force data can be interpolated for a desired number of spanwise and azimuthal discretization elements. An initial angle of attack at each of these elements is assumed and the inverse free wake model uses the normal and tangential forces to find the lift and drag components.

From the Kutta-Joukowski theorem a bound circulation distribution is obtained for every time step. From this, the trailed and shed circulation can be obtained. This enables the velocity field due to the turbine wake to be determined and the wake is allowed to develop freely under the influence of such a velocity field. A new angle of attack can thus be obtained which will enable a new circulation distribution to be obtained. This algorithm is shown schematically in Figure 4.

The process is repeated until a convergence in angle of attack is achieved. This is usually the case in two or three iterations. The process is an inverse free wake method because rather than obtaining the blade loads from two-dimensional airfoil information, it uses experimental measurements in order to solve for the velocity field and hence angles of attack on the rotor blades.

In the current work, C_n was analyzed instead of C_l for two reasons. First, C_n was considered a more physically pertinent parameter of interest because it decouples flow field activity from inflow direction. Second, adoption of C_n permits comparisons of results herein with a broad range of analyses previously accomplished for other experimental data.

With differences in rotor speed and blade chord length offsetting each other, Reynolds numbers for the UAE and MEXICO turbines were comparable, with both being on the order of 10^6. Angles of attack (α) for both the UAE and MEXICO experiments were computed using the same inverse free wake model, and so were consistent.

3.2 Mean C_n

Figure 5 shows mean C_n data corresponding to the farthest inboard radial locations on the MEXICO and UAE Phase VI blades. In the upper panel of Figure 5, UAE Phase VI mean C_n data acquired at 0.30R for stationary blade conditions are plotted as a function of α. Here, mean C_n initially increased linearly with α at a rate of 0.04 per degree. This slope was substantially lower than the 0.11 per degree rate for two-dimensional airfoils, indicating that three-dimensional influences were significant for this radial location under stationary blade conditions. Upon reaching α = 8.9º, the slope of the curve decreased visibly, but C_n continued to increase until α = 23.9º deg. At this point, C_n attained a maximum of 0.911 and stall occurred. Thereafter, C_n decreased slightly to a local minimum of 0.861 at 34.0º, and finally rose to C_n = 0.948 at 43.0º. MEXICO stationary blade data were not available for the 0.25R radial location.

The lower panel of Figure 5 shows mean C_n data acquired under rotating blade conditions on the MEXICO blade at 0.25R and the UAE blade at 0.30R. For both data sets, C_n increased with α in pseudo-linear fashion through the approximate range $0º \le \alpha \le 10º$, at a rate of 0.09 per degree. That this slope was more than twice that for the parked blade indicates that rotational influences began to modify the blade flow field at low α. At α = 8.9º for the MEXICO data and α = 10.7º for the UAE, curve slope decreased to less than half of its previous magnitude, but steepened again at $\alpha \approx 15º$, to 0.15 per degree for the MEXICO curve and 0.30 for the UAE. These C_n kinematics implied that exceeding the two-dimensional static stall α prompted significant rotational alterations to the blade flow field.

These exceptionally steep C_n–α curve subintervals culminated in C_n maxima (stall C_n), which occurred at α = 20.4º and C_n = 2.081 for MEXICO, and at α = 20.8º and C_n = 2.436 for the UAE. For both data sets, stall C_n was twice that generally observed for two-dimensional airfoils, and for the UAE was nearly three times that for the stationary blade. Rotating blade stall α was about 5º higher than that generally measured for two-dimensional airfoils, but for the UAE rotating blade stall α approximated stall α for the stationary blade. After reaching maximum (stall) C_n, MEXICO and UAE data displayed dramatically different kinematics. MEXICO C_n dropped precipitously from 2.081 to 1.564 over the α interval from 20.4º to 26.7º, and then remained approximately constant. In sharp contrast, UAE C_n declined gradually from 2.436 to 2.270 as α increased from 20.8º to 37.0º. Notably, neither inboard C_n–α curve exhibited a maximum, either absolute or local, in the α range commonly associated with two-dimensional airfoil stall. Rather, the only

maxima, corresponding to stall, occurred at α levels usually associated with airfoil post stall.

Figure 6 shows data for mid-radius stations on the MEXICO and UAE Phase VI blades. The upper panel of Figure 6, contains mean C_n–α data for the stationary MEXICO blade at 0.60R and for the stationary UAE blade at 0.63R. Through the range $0^o \le \alpha \le 14^o$, both curves followed highly similar trajectories. Both rose at the same slope of 0.08 per degree until reaching $\alpha = 8^o$. Thereafter, the slopes of both curves decreased progressively with increasing α, and both leveled off at $C_n = 1.04$ upon reaching $\alpha = 14^o$. At this point, the two curves diverged. The MEXICO curve decreased briefly to 0.737, and then rose sharply to a global maximum of $C_n = 1.185$ at $\alpha = 20.2^o$. Subsequently, MEXICO C_n decreased gradually to 0.848 at $\alpha = 30.2^o$, and then increased gradually to culminate at 0.971 at $\alpha = 45.2^o$. After diverging from the MEXICO curve, the UAE Phase VI curve decreased gradually to $C_n = 0.706$ at $\alpha = 27.1^o$, and finally increased in equally gradual fashion to end at 0.946, at $\alpha = 47.1^o$.

The lower panel of Figure 6 contains mean C_n data for rotating blade conditions on the MEXICO blade at 0.60R and on the UAE blade at 0.63R. For both data sets, C_n increased linearly with α until reaching $\alpha = 7.2^o$. In this low α range, the MEXICO and UAE C_n–α curve slopes were 0.11 and 0.08 per degree, respectively. As α increased beyond 7.2^o, C_n–α curve slopes decreased visibly for both MEXICO and UAE data. Subsequently, MEXICO C_n reached a maximum of 1.251 at $\alpha = 14.4^o$, and UAE C_n reached a maximum of 1.111 at $\alpha = 12.9^o$. These stall C_n values were higher by 8 percent and 6 percent, respectively, than those for the stationary blade C_n stall. MEXICO stall took place at marginally higher α and reached slightly higher C_n than that for the UAE. Nonetheless, stalling kinematics were highly similar for the two data sets, with C_n decreasing gradually after cresting at maximum (stall) levels. Notably, mid-radius MEXICO and UAE stall parameters (α and C_n) for the rotating blade did not differ radically from their stationary blade counterparts.

Though mid-radius stall kinematics differed little between the stationary and rotating blades, post-stall responses differed significantly between the stationary and rotating states. Following stall, UAE C_n declined to a local minimum of 0.935 at $\alpha = 15.5^o$. MEXICO C_n decreased to a slightly lower local minimum of 0.843, at a somewhat higher α of 22.6^o. After this, UAE C_n increased to an absolute maximum (post-stall) of 1.35 at $\alpha = 25.3^o$, and then declined slowly and nonmonotonically to culminate at $C_n = 1.249$ at $\alpha = 39.1^o$. MEXICO C_n increased from the local minimum for a brief interval, but halted prematurely at $\alpha = 26.6^o$, where $C_n = 1.006$.

3.3 Time Varying C_n

Figure 7 contains C_n standard deviation (σ_{Cn}) data for the farthest inboard radial locations on the MEXICO and UAE Phase VI blades. In the upper panel of Figure 7, UAE Phase VI σ_{Cn} data for 0.30R under stationary blade conditions are plotted as a function of α. Through the range $0^o \le \alpha \le 8.9^o$, σ_{Cn} remained constant at 0.017, and subsequently increased in linear fashion to a maximum of 0.059 at $\alpha = 18.9^o$. After attaining this maximum, σ_{Cn} decreased in intermittent steps over the next 30.0^o interval, and finally reached 0.020 at $\alpha = 48.9^o$. MEXICO stationary blade data were not available for the 0.25R radial location.

The lower panel of Figure 7 shows σ_{Cn} data acquired under rotating blade conditions on the MEXICO blade at 0.25R and the UAE blade at 0.30R. In the low α range, σ_{Cn} remained low and approximately level for both the MEXICO and UAE data. Upon reaching $\alpha = 15.0$ deg, the MEXICO σ_{Cn} began to rise at a modest rate until $\alpha = 20.4^o$. Over approximately the same α interval, UAE σ_{Cn} increased sharply after $\alpha = 13.3^o$, reaching a local maximum of 0.178 at $\alpha = 17.8^o$.

Beyond $\alpha = 20.4^o$, higher α prompted relatively small though visible variations in MEXICO σ_{Cn}, with the lowest σ_{Cn} in this α range being 0.072 at $\alpha = 37.7^o$, and the highest being 0.091 at $\alpha = 48.5^o$. Over a comparable range of $19.7^o \le \alpha \le 30.2^o$, UAE σ_{Cn} climbed to a maximum of $\sigma_{Cn} = 0.214$ at $\alpha = 30.2^o$, though the σ_{Cn} rate of increase through $19.7^o \le \alpha \le 30.2^o$ was significantly lower than that over $13.3^o \le \alpha \le 17.8^o$. Though the σ_{Cn} magnitudes observed for the UAE σ_{Cn} were appreciably higher than those for MEXICO, the two curves were well correlated with respect to slope variations and the occurrence of minima and maxima.

Figure 8 contains C_n standard deviation (σ_{Cn}) data for the mid-radius locations on the MEXICO and UAE Phase VI blades. In Figure 8, the upper panel contains σ_{Cn} data for the stationary MEXICO blade at 0.60R and for the stationary UAE blade at 0.63R. Clearly, the two σ_{Cn}–α curves show striking similarities with respect to maximal magnitudes and slope correlations. Through the range $0.0^o \le \alpha \le 12.2^o$, neither

curve deviated significantly from the other, with both remaining constant at σ_{Cn} = 0.01. After α = 12.2º, both curves began to rise at moderate and similar rates, with the MEXICO curve peaking at σ_{Cn} = 0.060 at α = 18.2º, and the UAE curve peaking at σ_{Cn} = 0.057 and α = 22.1º. During the subsequent decrease in σ_{Cn}, the two curves continued to resemble each other, with the MEXICO curve reaching a minimum of σ_{Cn} = 0.038 at α = 30.2º, and the UAE curve doing the same at σ_{Cn} = 0.032 and α = 27.1º. Thereafter, at higher values of α, the correlation between the two curves was less evident, though still perceptible.

The lower panel of Figure 8 shows σ_{Cn} data acquired during blade rotation from the MEXICO blade at 0.60R and the UAE blade at 0.62R. Like the stationary blade data in the upper panel of Figure 8, the data for the MEXICO and UAE rotating blades show remarkable similarities. Below α = 10º, σ_{Cn} remains below 0.01 for 15 of 16 data points in this range. The sole exception is the UAE data point at α = 3.2º, which assumes a value of 0.015. At approximately α = 10º, both the MEXICO and UAE curves begin to rise rapidly. Shortly thereafter, at α = 19.2º, the MEXICO curve peaks at σ_{Cn} = 0.125, and at α = 18.2º, the UAE curve peaks at σ_{Cn} = 0.189.

From this peak, the MEXICO curve decreases to σ_{Cn} = 0.076 at α = 22.6º, and then rises to culminate at σ_{Cn} = 0.094 at α = 26.6º. Similarly, from the UAE peak, the curve descends to σ_{Cn} = 0.146 at α = 22.1º, and then rises again, reaching σ_{Cn} = 0.165 at α = 27.0º. Though the MEXICO data end at α = 26.6º and the UAE data continue through α = 39.1º, the correlation between the two data sets through the range 0º ≤ α ≤ 27º is dramatic. This implies correspondingly prominent similarities in the unsteady flow physics of the MEXICO and UAE blades near mid-radius.

3.4 Sectional c_p Distributions

Blade c_p data were analyzed to better understand the fluid dynamics responsible for the MEXICO and UAE C_n kinematics. Specifically, MEXICO and UAE Phase VI mean sectional c_p distributions, for rotating blade stall conditions, were compared at the inboard and mid-radius locations.

The MEXICO rotating blade c_p data shown in Figure 9 were acquired at 0.25R for α = 20.4º. The MEXICO suction surface c_p distribution had a suction peak at 0.002c where c_p = -7.496. Aft of this peak, c_p magnitude decreased sharply over the leading 0.11c, then more gradually from 0.11c to 0.30c, and finally became virtually constant on the aft 0.70c of the suction surface. Over the aft 0.70c, c_p varied between -0.935 and -1.461. On the MEXICO blade pressure surface, stagnation was detected at the 0.16c tap location.

Also shown in Figure 9 are UAE rotating blade c_p data, which were measured at 0.30R for α = 20.8º. UAE suction surface c_p exhibited no leading edge suction peak, and instead assumed a virtually constant level of approximately -2.5 over the chord range 0.0c ≤ x/c ≤ 0.56c . Aft of 0.56c, c_p level varied in pseudo-linear fashion, reaching c_p = -0.394 at the trailing edge. On the UAE blade pressure surface, stagnation was detected at the 0.06c tap location.

Notably, the Figure 9 MEXICO and UAE rotating blade stall c_p distributions differed dramatically from each other, even though they were measured at nearly identical α and yielded stall C_n levels that were comparably elevated (Figure 5). Thus, it was evident that different c_p distribution features were responsible for observed C_n amplifications. Though the MEXICO and UAE pressure surface c_p distributions were slightly unconventional, none of the attributes present there could account for the C_n amplifications, thus focusing attention on the suction surface.

The MEXICO suction surface c_p distribution displayed two attributes that differed appreciably from stationary airfoils. First, while suction peak height was not significantly greater than that observed on stationary airfoils, suction peak chordwise extent was substantially broader. Second, c_p values of -0.935 to -1.461 in the 0.30c ≤ x/c ≤ 1.0c chord region were two to three times greater than those produced by stationary airfoils. In contrast, the entire UAE suction surface was nonstandard in conformation and was augmented in c_p magnitude, and was responsible for amplifying C_n. As shown in previous research, these contrasting c_p distributions imply conspicuously different flow field topologies.[15,16] The Figure 9 MEXICO c_p distribution is consistent with a flow field containing a trailing edge separation, while c_p distributions like that for the UAE have been linked to leading edge separation and downstream shear layer impingement.

Figure 10 shows rotating blade c_p data for the MEXICO blade at 0.60R, and for the UAE blade at 0.63R. The MEXICO data correspond to α = 14.4º and the UAE data to α = 12.9º, both of which represent stall conditions consistent with the rotating blade data in Figure 6. Both c_p

distributions are highly conventional, and strongly resemble those for stationary airfoils. Specifically, both the MEXICO and UAE pressure distributions have very narrow suction peaks, with minimum c_p values of -5.816 and -3.874. From 0.02c to midchord, c_p magnitudes for both blades decrease gradually until reaching the midchord. Between midchord and trailing edge, c_p for both blades remains virtually constant at -0.3 to -0.4, again similar to stationary airfoils. The c_p distributions in Figure 10 both are consistent with trailing edge separation [15,16], and significant augmentation relative to stationary airfoil c_p distributions is not evident.

While Figure 10 data represented mid-radius stall, Figure 11 contains c_p distributions for mid-radius post-stall conditions on the MEXICO and UAE rotating blades. The Figure 11 UAE c_p distribution corresponds to the Figure 6 UAE C_n maximum of 1.35 at α = 25.3º. The Figure 11 MEXICO c_p distribution corresponds to the final data point in the Figure 6 MEXICO curve, where α = 26.6º and C_n = 1.006. As shown in Figure 11, suction peaked near the leading edges, where c_p values were -1.182 for MEXICO and -1.436 for the UAE. Proceeding aft on the blade chord, c_p magnitude decreased slowly for both the MEXICO and UAE, yielding nearly level c_p distributions. Relative to c_p magnitudes commonly associated with stalled two-dimensional airfoils, MEXICO c_p magnitudes were marginally greater, while UAE c_p magnitudes were appreciably larger. Notably, the Figure 11 UAE mid-radius cp distribution was strongly reminiscent of the UAE inboard c_p distribution in Figure 9. Consistent with the rest of the current work, pressure surface c_p distributions in Figure 11 strongly resembled those of stationary two-dimensional airfoils.

3.5 Planform Pressure Topologies

To analyze flow field kinematics over the entire blade in more cohesive fashion, surface pressures (not c_p) were contour plotted over the blade suction surface. Operating conditions at or near stalled operation were selected for analysis. Time records of c_p data were time averaged over the entire data set, and the resulting mean c_p data were converted to dimensional pressures (Pascals) referenced to test section static pressure. The results are shown in Figures 12 and 13.

Figure 12 shows surface pressure contours on the MEXICO blade for U_∞ = 19.8 m/s. Contours were plotted using all suction surface pressure taps at r/R = 0.25, 0.35, 0.60, 0.82, and 0.92. Pressure contour interval (Δp) is 500 Pa. Lowest pressures were observed at the leading edge nearest the blade tip. Moving along the blade leading edge from 0.92R to 0.35R resulted in progressively higher pressure levels. Once maximum pressure was reached at 0.35R, further inboard movement along the leading edge produced lower pressure levels. Contours showed that surface pressures at r/R = 0.60, 0.82, and 0.92 increased steeply over the forward half chord, and then underwent little change over the remaining aft chord. This same trend was evident at 0.25R, although steep pressure increases were confined to the forward quarter chord, with little apparent change aft of there. The 0.35R location differed fundamentally from the other four radial stations, in that surface pressures remained level over the entire blade chord.

Figure 13 shows UAE blade surface pressure contours corresponding to U_∞ = 15.1 m/s. Contour plots include data from all suction surface pressure taps at r/R = 0.30, 0.47, 0.63, 0.80, and 0.95. Pressure contour interval (Δp) is 100 Pa. As for the MEXICO blade, lowest pressures were observed at the blade leading edge nearest the tip. Progressing along the blade leading edge from 0.95R to 0.80R yielded steep pressure increases. Further movement inboard from 0.80R to 0.47R continued to produce pressure increases, though at a slower rate of growth. This trend reversed from 0.47R to 0.30R, in which leading edge surface pressure decreased. Along the chordwise direction, contours showed that surface pressures at 0.95R increased steeply over the forward quarter chord, and then exhibited negligible change aft of this location. At r/R = 0.80, 0.63, and 0.30, surface pressures increased in approximate linear fashion from leading to trailing edge. Analogous to the MEXICO blade at 0.35R, the UAE 0.47R location differed fundamentally from the other four radial stations. Here, surface pressures appeared approximately level from leading to trailing edge.

Though obscured by MEXICO and UAE planform differences, careful comparisons revealed that the two pressure topologies were congruent in two key respects. First, along the spanwise direction, surface pressures attained maxima at locations just inboard of mid-radius, and decreased both inboard and outboard of there. Second, at this maximal pressure span location, chordwise surface pressures were level, while chordwise pressure distributions at other radial locations displayed significant variation.

4 Conclusions

The MEXICO and UAE Phase VI and experiments were complementary in many crucial respects, and thus offer unprecedented synergies to better understand and predict rotational augmentation of blade aerodynamics. Comparisons of the two surface pressure data sets included both C_n mean and C_n standard deviation statistics and encompassed stationary blade baseline data as well as rotating blade data. Angles of attack were computed for both data sets using the same validated inverse free wake model, which provided an accurate and consistent inflow reference. Analyses of inboard and mid-radius blade locations presented herein support the following conclusions.

- Rotational effects on mean C_n are active across the entire blade performance envelope. At low and moderate α where inviscid influences dominate, blade rotation steepens C_n–α curves. At elevated α where viscous effects play a major role, blade rotation delays stall to higher α, and produces higher stall C_n.
- At each radial location, MEXICO and UAE C_n–α curve steepening, stall α delay, and C_n amplification are closely comparable. However, as indicated by C_n–α curve conformation in the stall and post-stall α range, MEXICO and UAE stall dynamics differ appreciably for inboard locations and to a lesser extent at mid-radius, consistent with differences in respective airfoil shapes.
- Consistent with disparate inboard C_n–α curves, inboard c_p distributions also are dissimilar. The MEXICO c_p distribution is consistent with a trailing edge separation, while the UAE distribution implies a leading edge separation followed by shear layer impingement.
- Blade rotation amplifies C_n standard deviation levels above those for stationary blades. UAE C_n standard deviation levels consistently exceed those for MEXICO. However, strong correlations exist between MEXICO and UAE C_n standard deviation level variations with respect to α.
- The MEXICO and UAE blade planforms differ substantially. Nonetheless, three-dimensional surface pressure topologies corresponding to peak stall operation share common features, testifying to the robustness of the rotationally modified flow field.

The current work has comparatively analyzed MEXICO and UAE data to validate and generalize knowledge regarding rotationally augmented blade flow fields. Some results presented herein provide confirmation of prior research, while other results provide insights not previously grasped in analyses of either data set alone. Future inquiry using the MEXICO and UAE data will foster more complete understanding of rotationally augmented blade flows, and thus facilitate more accurate prediction and improved turbine design.

5 References

[1] Schepers, J. G., Brand, A., Bruining, A, Graham, J., Hand, M., Infield, D., Madsen, H., Paynter, J., Simms, D., “Final Report of IEA Annex XIV: Field Rotor Aerodynamics”, ECN-C--97-027, Energy Research Centre of The Netherlands, Petten, The Netherlands, June 1997.

[2] Schepers, J. G., Brand, A., Bruining, A, Hand, M., Infield, D., Madsen, H., Maeda, T., Paynter, J., van Rooij, R., Shimizu, Y., Simms, D., and Stefanatos, N., “Final Report of IEA Annex XVIII: Enhanced Field Rotor Aerodynamics Database”, ECN-C--02-016, Energy Research Centre of The Netherlands, Petten, The Netherlands, February 2002.

[3] Dexin, H., and Thor, S.-E., “The Execution of Wind Energy Projects 1986-1992,” FFA TN 1993-19, Aeronautical Research Institute of Sweden, Bromma, June 1993.

[4] Ronsten, G., “Geometry and Installation of Wind Tunnels of a STORK 5.0 WPX Wind Turbine Blade Equipped with Presssure Taps,” FFAP-A 1006, Aeronautical Research Institute of Sweden, Bromma, February 1994.

[5] Hand, M., Simms, D., Fingersh, L., Jager, D., Cotrell, J., Schreck, S., and Larwood, S., “Unsteady Aerodynamics Experiment Phase VI: Wind Tunnel Test Configurations and Available Data Campaigns,” NREL/TP-500-29955, December 2001, Golden, CO: National Renewable Energy Laboratory.

[6] Snel, H., Schepers, J., and Montgomerie, B., “The MEXICO project (Model Experiments in Controlled Conditions): The database and first results of data processing and interpretation,” The Science of Making Torque from Wind Conference, Journal of Physics: Conference Series **75** (2007) 012014 doi:10.1088/1742-6596/75/1/012014.

[7] Schreck, S., “Low Frequency Shedding Prompted by Three-Dimensionality under Rotational Augmentation,” AIAA-2010-0640, January 2010.

[8] Snel, H., J. Schepers, and B. Montgomerie, 2007, “The MEXICO project

(Model Experiments in Controlled Conditions): The Database and First Results of Data Processing and Interpretation," The Science of Making Torque from Wind Conference, *Journal of Physics: Conference Series 75*.
[9] Snel, H., Schepers, G., and Siccama, N., "MEXICO Project: The Database and Results of Data Processing and Interpretation," AIAA-2009-1217, January 2009.
[8] Giguere, P., and M. Selig, "Design of a Tapered and Twisted Blade for the NREL Combined Experiment Rotor," NREL/SR 500-26173, Apr. 1999, Golden, CO: National Renewable Energy Laboratory.
[9] Butterfield, C., W. Musial, and D. Simms, (1992). "Combined Experiment Phase I Final Report" NREL/TP-257-4655. Golden, CO: National Renewable Energy Laboratory.
[10] Zell, P., "Performance and Test Section Flow Characteristics of the National Full-Scale Aerodynamics Complex 80- by 120-Foot Wind Tunnel," NASA TM 103920, January 1993.
[11] Snel, H., J. Schepers, and B. Montgomerie, 2007, "The MEXICO project (Model Experiments in Controlled Conditions): The Database and First Results of Data Processing and Interpretation," The Science of Making Torque from Wind Conference, *Journal of Physics: Conference Series 75*.
[12] Snel, H., Schepers, G., and Siccama, N., "MEXICO Project: The Database and Results of Data Processing and Interpretation," AIAA-2009-1217, January 2009.
[13] Sant T., van Kuik G. and van Bussel G. J. W., "Estimating the angle of attack from blade pressure measurements on the NREL Phase VI rotor using a free wake vortex model: axial conditions," *Wind Energy*, v. 9, n. 6, pp. 549 – 577, 2006.
[14] Micallef, D., Kloosterman, M., Ferreira, C., Sant, T., and van Bussel G.J.W., "Validating BEM, Direct and Inverse Free Wake Models with the MEXICO Experiment," AIAA-2010-0462, January 2010.
[15] Schreck, S., and Robinson, M., "Boundary Layer State and Flow Field Structure Underlying Rotational Augmentation of Blade Aerodynamic Response," *J. of Solar Energy Eng.*, v. 125, pp. 448-456, November 2003.
[16] Schreck, S., Sørensen, N., and Robinson, M., "Aerodynamic Structures and Processes in Rotationally Augmented Flow Fields," *Wind Energy*, v. 10, n. 2, March/April 2007, pp. 159-178.

Figure 1. MEXICO turbine mounted in DNW 9.5 m x 9.5 m wind tunnel (left) and UAE Phase VI turbine mounted in NASA Ames 24.4 m x 36.6 m wind tunnel (right).

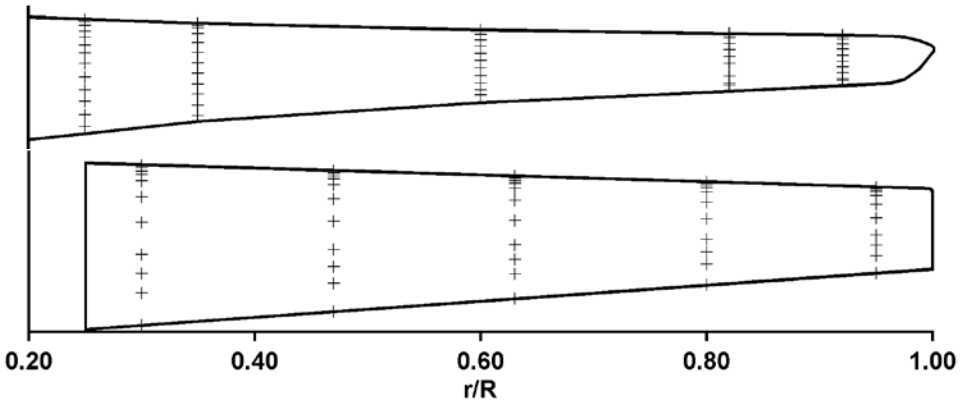

Figure 2. MEXICO and UAE Phase VI blade planform drawings with suction surface tap locations. Leading edge is at the top of each planform.

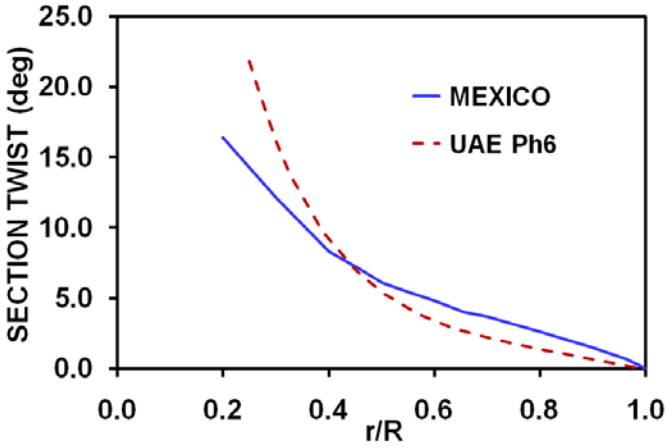

Figure 3. Sectional blade twist for aerodynamically active parts of MEXICO and UAE Phase VI blades.

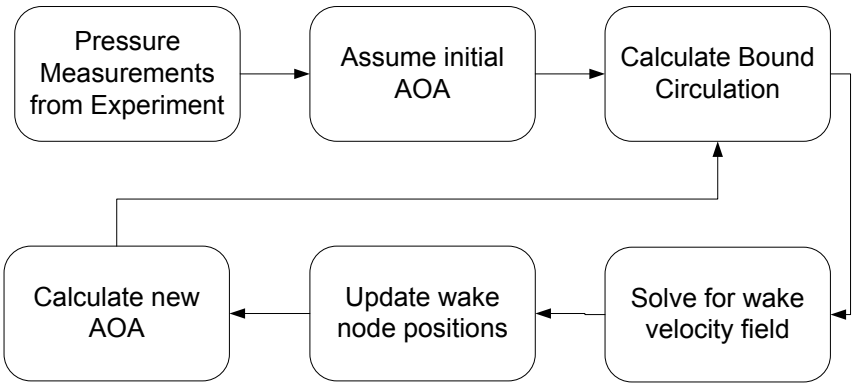

Figure 4. Schematic of inverse free wake model algorithm used to compute angles of attack for MEXICO and UAE Phase VI data.

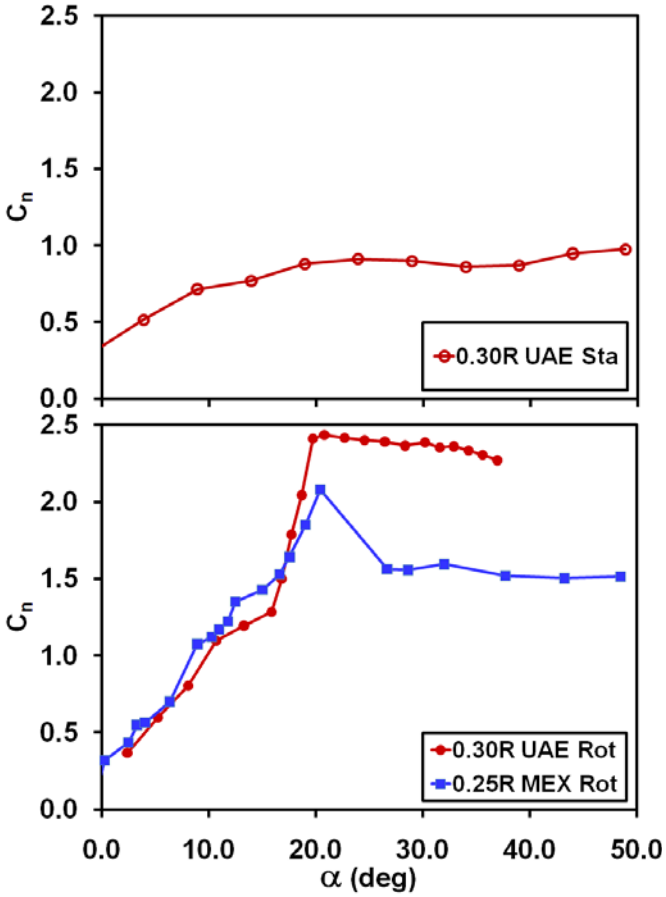

Figure 5. MEXICO and UAE Phase VI mean C_n at inboard radius, for parked (upper panel) and rotating (lower panel) blades.

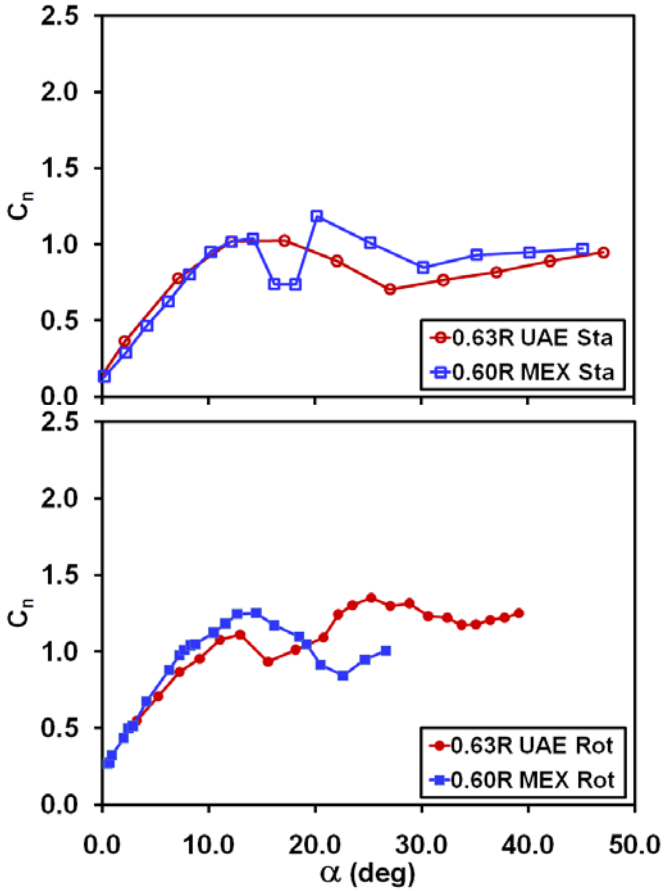

Figure 6. MEXICO and UAE Phase VI mean C_n at mid-span radius, for parked (upper panel) and rotating (lower panel) blades.

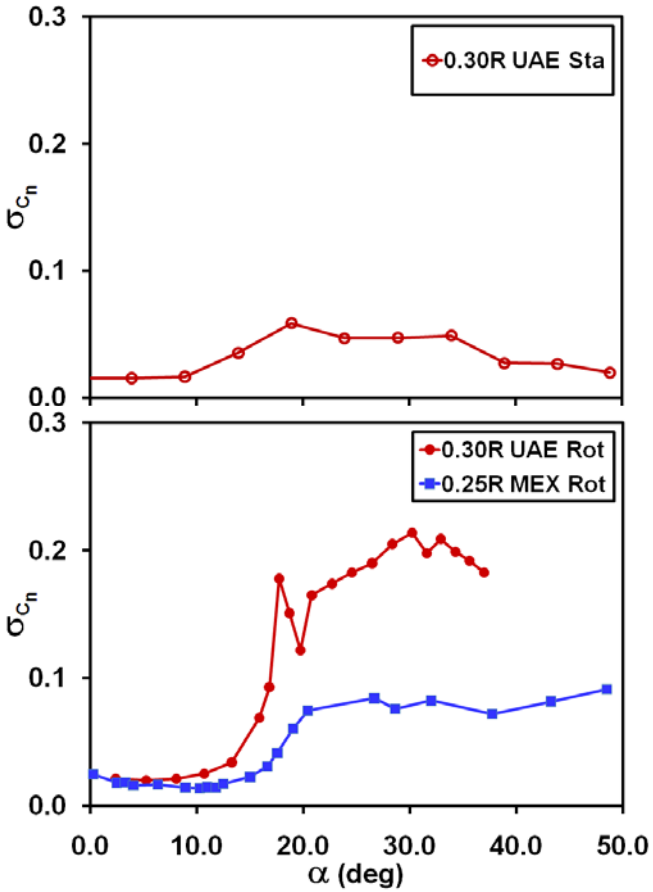

Figure 7. MEXICO and UAE Phase VI σ_{Cn} at inboard radius, for parked (upper panel) and rotating (lower panel) blades.

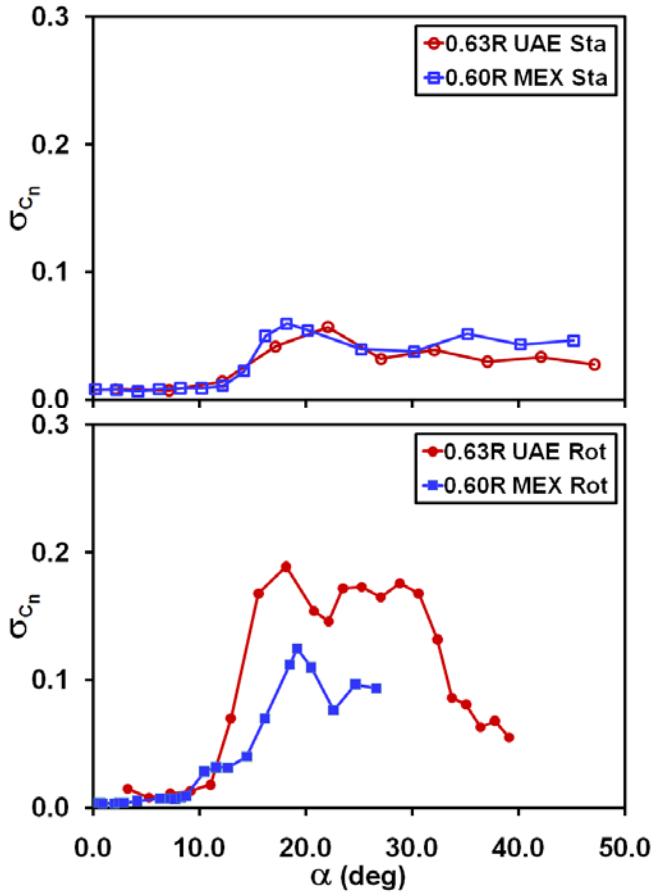

Figure 8. MEXICO and UAE Phase VI σ_{Cn} near mid-span radius, for parked (upper panel) and rotating (lower panel) blades.

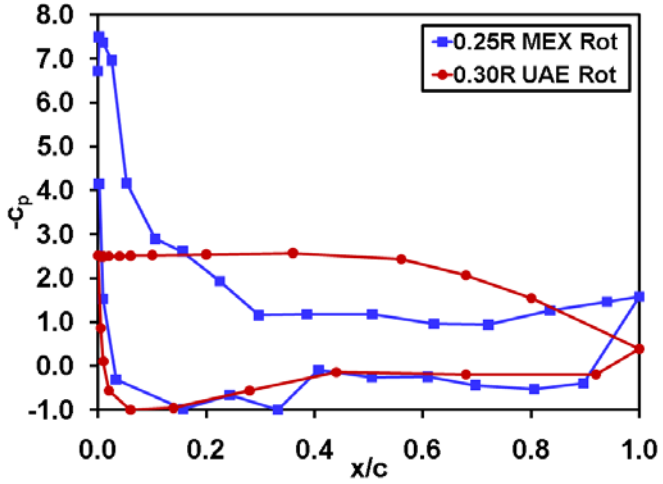

Figure 9. MEXICO and UAE Phase VI stall c_p distributions at inboard radius, for rotating blades. MEXICO $\alpha = 20.4^o$ and UAE $\alpha = 20.8^o$.

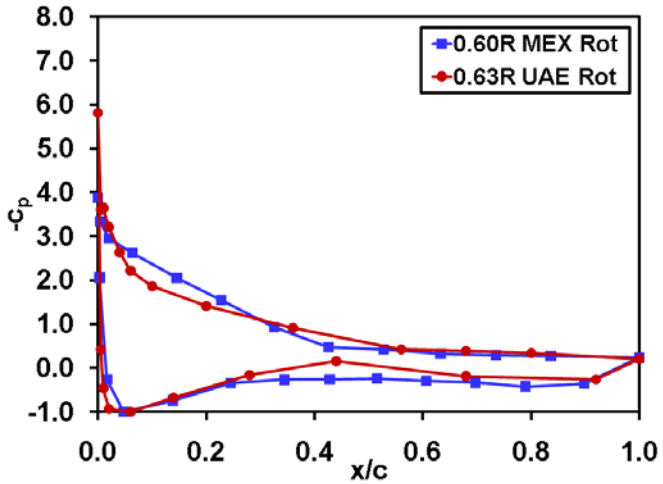

Figure 10. MEXICO and UAE Phase VI stall c_p distributions near mid-span radius, for rotating blades. MEXICO $\alpha = 14.4^o$ and UAE $\alpha = 12.9^o$.

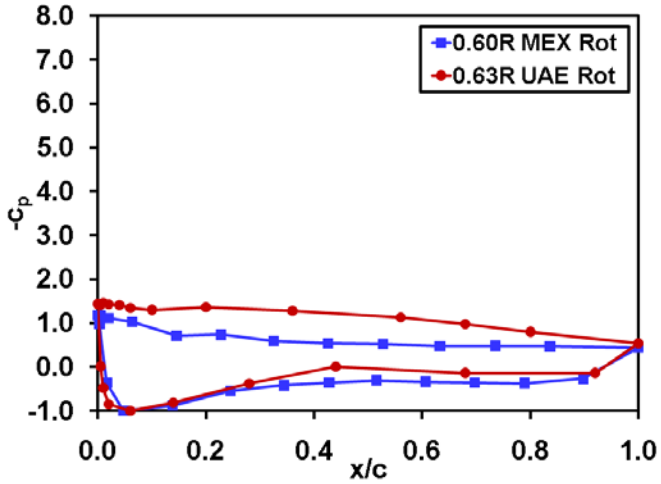

Figure 11. MEXICO and UAE Phase VI post-stall c_p distributions near mid-span radius, for rotating blades. MEXICO $\alpha = 26.6^o$ and UAE $\alpha = 25.3^o$.

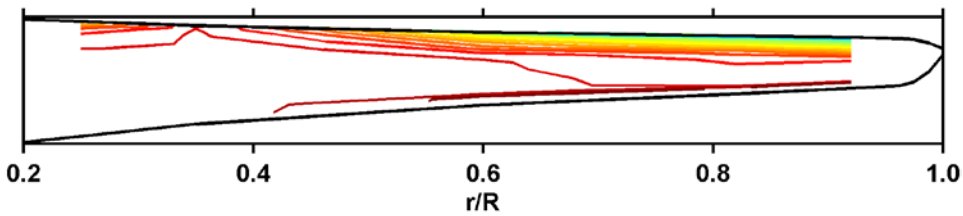

Figure 12. MEXICO suction surface pressure contours. U_∞ = 19.8 m/s, contour Δp = 500 Pa. Leading edge is at the top of planform.

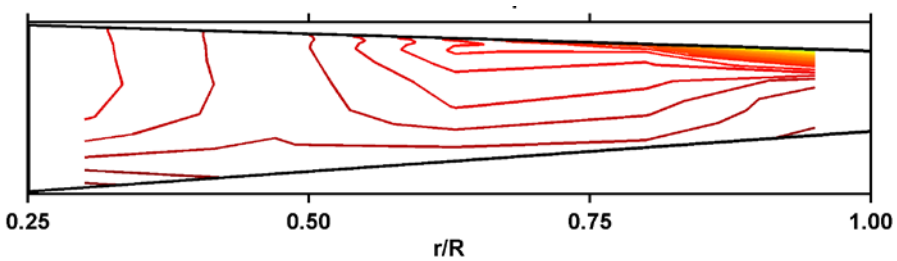

Figure 13. UAE Phase VI suction surface pressure contours. U_∞ = 15.1 m/s, contour Δp = 100 Pa. Leading edge is at the top of planform.

REPORT DOCUMENTATION PAGE

Form Approved
OMB No. 0704-0188

PLEASE DO NOT RETURN YOUR FORM TO THE ABOVE ORGANIZATION.

1. REPORT DATE *(DD-MM-YYYY)*	2. REPORT TYPE	3. DATES COVERED *(From - To)*
May 2010	Conference Paper	June 28-30,2010

4. TITLE AND SUBTITLE
Rotational Augmentation Disparities in the MEXICO and UAE Phase VI Experiments: Preprint

5a. CONTRACT NUMBER
DE-AC36-08-GO28308

5b. GRANT NUMBER

5c. PROGRAM ELEMENT NUMBER

6. AUTHOR(S)
S. Schreck, T. Sant, and D. Micallef

5d. PROJECT NUMBER
NREL/CP-500-47759

5e. TASK NUMBER
WE103111

5f. WORK UNIT NUMBER

7. PERFORMING ORGANIZATION NAME(S) AND ADDRESS(ES)
National Renewable Energy Laboratory
1617 Cole Blvd.
Golden, CO 80401-3393

8. PERFORMING ORGANIZATION REPORT NUMBER
NREL/CP-500-47759

9. SPONSORING/MONITORING AGENCY NAME(S) AND ADDRESS(ES)

10. SPONSOR/MONITOR'S ACRONYM(S)
NREL

11. SPONSORING/MONITORING AGENCY REPORT NUMBER

12. DISTRIBUTION AVAILABILITY STATEMENT
National Technical Information Service
U.S. Department of Commerce
5285 Port Royal Road
Springfield, VA 22161

13. SUPPLEMENTARY NOTES

14. ABSTRACT *(Maximum 200 Words)*

Wind turbine structures and components suffer excessive loads and premature failures when key aerodynamic phenomena are not well characterized, fail to be understood, or are inaccurately predicted. Turbine blade rotational augmentation remains incompletely characterized and understood, thus limiting robust prediction for design. Pertinent rotational augmentation research including experimental, theoretical, and computational work has been pursued for some time, but large scale wind tunnel testing is a relatively recent development for investigating wind turbine blade aerodynamics. Because of their large scale and complementary nature, the MEXICO and UAE Phase VI wind tunnel experiments offer unprecedented synergies to better characterize and understand rotational augmentation of blade aerodynamics.

15. SUBJECT TERMS
Force amplification; rotational augmentation; wind tunnel; wind turbine; unsteady loading

16. SECURITY CLASSIFICATION OF:			17. LIMITATION OF ABSTRACT	18. NUMBER OF PAGES	19a. NAME OF RESPONSIBLE PERSON
a. REPORT	b. ABSTRACT	c. THIS PAGE			19b. TELEPHONE NUMBER (*Include area code*)
Unclassified	Unclassified	Unclassified	UL		

Standard Form 298 (Rev. 8/98)
Prescribed by ANSI Std. Z39.18

F1147-E(10/2008)